Journal of Computational and Applied Mathematics 448 (2024) 115896

Contents lists available at ScienceDirect

Journal of Computational and Applied Mathematics

journal homepage: www.elsevier.com/locate/cam

Multinode Shepard method for two-dimensional elliptic boundary problems on different shaped domains

Francesco Dell'Accio [a,*], Filomena Di Tommaso [a], Elisa Francomano [b]

[a] Department of Mathematics and Computer Science, University of Calabria, Via P. Bucci, Rende (CS), Italy
[b] Department of Engineering, University of Palermo, Viale delle Scienze, Palermo, Italy

ARTICLE INFO

Keywords:
Approximation by rational functions
Multinode Shepard method
Collocation method
Elliptic PDEs

ABSTRACT

In this paper, we continue the study on the application of multinode Shepard method to numerically solve elliptic Partial Differential Equations (PDEs) equipped with various conditions at the boundary of domains of different shapes. In particular, for the first time, the multinode Shepard method is proposed to solve elliptic PDEs with Dirichlet and/or Neumann boundary conditions. The method has been opportunely handled to efficiently work dealing with scattered distribution of points and, to this aim, several experiments in different 2d domains have been performed. Comparisons with the analytic solution and the results generated by the Kansa's RBF solvers have been reported referring to Halton points. The results are very promising and should be of interest for applications in the real world.

1. Introduction

As well known, every field in science and engineering uses models based on differential equations: from biology to medicine, from physics to chemistry, and all engineering sciences. Despite the huge number of known Partial Differential Equations (PDEs), continuously discovered in modeling new problems, only a few possess closed-form solutions and numerical methods allow to represent such solutions with the help of adequate designed software [1].

Elliptic PDEs are special kinds of second-order equations, which find applications in almost all areas of mathematics, from harmonic analysis to geometry to Lie theory, as well as numerous applications in physics, and they have a well-developed theory. The Laplacian operator, in particular, is a fundamental component in a large number of multi-dimensional linear models of mathematical physics: to name a few, the Laplacian arises in descriptions of various classical and quantum wave phenomena, as well as models involving diffusion and viscosity effects [2].

Often the elliptic PDEs are coupled with boundary conditions, to define a boundary value problem in which the solution of the given equation is required to satisfy conditions, such as Dirichlet or Neumann conditions or mixed ones, on the boundary of the problem domain.

The most popular numerical methods for solving PDEs are finite difference methods (FDMs), spectral methods, finite element methods (FEMs), boundary element methods (BEMs), finite volume methods (FVMs). Despite their popularity, classical methods based on local polynomial interpolation, have low algebraic convergence rates. On the other hand, global polynomial methods, have exponential convergence rates, but in any case a structured grid is required. Radial basis functions (RBFs) [3–5] have been adopted into the PDEs framework too [6–8]. The direct use of RBFs to solve PDEs via collocation was first attempted by Kansa in 1990 [6]

* Corresponding author.
E-mail addresses: francesco.dellaccio@unical.it (F. Dell'Accio), filomena.ditommaso@unical.it (F. Di Tommaso), elisa.francomano@unipa.it (E. Francomano).

https://doi.org/10.1016/j.cam.2024.115896
Received 30 October 2023; Received in revised form 6 February 2024
Available online 2 April 2024

and widely used in the applications. In this method, multiquadric RBFs were used to approximate the solution, and point collocation was considered to enforce the governing equation and boundary conditions [9]. In the last years, it has been also investigated a generalization of the Kansa method, called *polynomial-augmented RBF*, which consists of adding multivariate polynomials to the RBF basis, and then imposing matching constraints [10,11]. This approach increases the accuracy of the approximation by high-degree polynomials and stabilizes the system through the RBFs [12]. The RBFs collocation methods do not require a grid and are powerful when one has to work with irregular domains [13–17]. The disadvantages are that often the condition number of the collocation matrix is too large and severe ill-conditioning results [18]. As shown in recent works [19,20], these drawbacks do not occur in using the multinode Shepard (MS) method, instead of the RBFs, in collocation.

In this paper, we continue our studies on the possible application of the MS method to solve elliptic PDEs with Dirichlet or mixed boundary conditions by considering domains of different shapes in 2d. In order to maintain the paper self-contained, we briefly outline the main features of the MS method in Section 2. In Section 3, the MS method is used to efficiently solve different elliptic PDEs, with Dirichlet boundary conditions, dealing with scattered distribution of points, and comparisons with the analytic solution and the results provided by Kansa's RBFs solver are reported. Similar experiments, using Halton points, have been conducted in Section 5 for the case of elliptic PDEs with mixed boundary conditions. Finally, Section 6 is devoted to conclusions and further perspective of work.

2. A brief overview on the multinode Shepard method

To maintain the paper self-contained, in this section, we shortly describe the MS method, which is the main ingredient of the adopted numerical approach. The MS method is an accurate procedure for reconstructing functions from scattered data, which arises by combining local interpolation polynomials of a fixed degree with inverse distance weighted basis functions [19].

Let $\Omega \subset \mathbb{R}^d$, $d \geq 2$, be a region (i.e. a non-empty connected open set), $\partial\Omega$ its boundary, $\Xi = \{\boldsymbol{\xi}_i\}_{i=1}^n \subset \Omega \cup \partial\Omega$ a finite set of pairwise distinct scattered nodes and $f = \{f_i\}_{i=1}^n$ the associated function values. Let $r \in \mathbb{N}$ and $m = \binom{r+d}{d} = \dim\left(\mathcal{P}_r(\mathbb{R}^d)\right)$, where $\mathcal{P}_r(\mathbb{R}^d)$ denotes the space of polynomials of d variables of total degree $\leq r$.

We assume that a set $\{\sigma_j\}_{j=1}^s$ is given, such that for each $j = 1, \dots, s$, $\sigma_j = \{\boldsymbol{\xi}_{j_i}\}_{i=1}^m \subset \Xi$ is unisolvent for the polynomial space $\mathcal{P}_r(\mathbb{R}^d)$ and

$$\bigcup_{j=1}^{s} \sigma_j = \Xi \tag{1}$$

(to shorten the notation, for each $j = 1, \dots, s$, we are denoting with $j_\imath = \varphi_j(\imath)$ the image of $\imath \in \{1, \dots, m\}$ by an injective map φ_j from $\{1, \dots, m\}$ into $\{1, \dots, n\}$).

A convenient way to represent the unique polynomial $P_j \in \mathcal{P}_r(\mathbb{R}^d)$, $j = 1, \dots, s$ interpolating on $\sigma_j = \{\boldsymbol{\xi}_{j_1}, \dots, \boldsymbol{\xi}_{j_m}\}$ the data $\{f_{j_1}, \dots, f_{j_m}\}$ is as follows

$$P_j(\boldsymbol{x}) = \sum_{\imath=1}^{m} \ell_{j,\imath}(\boldsymbol{x}) f_{j_\imath}, \qquad \boldsymbol{x} \in \mathbb{R}^d,$$

where

$$\ell_{j,\imath}(\boldsymbol{x}) = \sum_{|\alpha| \leq r} a_\alpha^{(j,\imath)} \left(\boldsymbol{x} - \boldsymbol{\xi}_j^{(b)}\right)^\alpha,$$

are the Lagrange fundamental polynomials written in the Taylor basis centered at the barycenter $\boldsymbol{\xi}_j^{(b)}$ of σ_j and $\alpha \in \mathbb{N}^m \cup \{(0, \dots, 0)\}$ is a multi-index (for more details see [21]). It is a well-known fact that

$$\ell_{j,\imath}\left(\boldsymbol{\xi}_{j_\kappa}\right) = \delta_{\imath\kappa}, \quad j = 1, \dots, s, \ \imath, \kappa = 1, \dots, m. \tag{2}$$

The existence of a covering $\left\{\sigma_j\right\}_{j=1}^s$ of Ξ is *almost surely* guaranteed [22]. In [19] we detailed a procedure to determine such a covering which consists of considering, for each scattered point $\boldsymbol{\xi}_i$, the set of $m + q$, $q > 0$, nearest points and in choosing, among them, the subset of m discrete Leja points computed by the algorithm presented in [23]. In terms of computational cost and accuracy of the results, such a procedure can be much improved by minimizing the number s of elements of the covering $\left\{\sigma_j\right\}_{j=1}^s$. In the numerical experiments, we make use of the improved procedure.

The multinode inverse distance weighted basis functions based on the covering $\{\sigma_j\}_{j=1}^s$ are defined as follows [24]

$$W_{\mu,j}(\boldsymbol{x}) = \frac{\prod_{\imath=1}^{m} \left\|\boldsymbol{x} - \boldsymbol{\xi}_{j_\imath}\right\|^{-\mu}}{\sum_{l=1}^{s} \prod_{\lambda=1}^{m} \left\|\boldsymbol{x} - \boldsymbol{\xi}_{l_\lambda}\right\|^{-\mu}}, \qquad j = 1, \dots, s,$$

where $\mu > 0$ is fixed. They are a partition of unity

$$\sum_{j=1}^{s} W_{\mu,j}(\boldsymbol{x}) = 1, \quad \boldsymbol{x} \in \mathbb{R}^d, \tag{3}$$

and satisfy the following interpolation properties

$$W_{\mu,j}\left(\boldsymbol{\xi}_i\right) = 0 \text{ for all } \boldsymbol{\xi}_i \notin \sigma_j, \quad \sum_{j \in \mathcal{J}_i} W_{\mu,j}\left(\boldsymbol{\xi}_i\right) = 1, \tag{4}$$

where we set

$$\mathcal{J}_i = \{j \in \{1, \dots, s\} : \boldsymbol{\xi}_i \in \sigma_j\}, \quad i = 1, \dots, n.$$

In addition, if $\mu > 2$ the multinode basis functions $W_{\mu,j}(\boldsymbol{x})$ satisfy the following differential properties

$$\nabla W_{\mu,j}(\boldsymbol{\xi}_i) = \mathbf{0} \text{ for all } \boldsymbol{\xi}_i \notin \sigma_j, \quad \sum_{j \in \mathcal{J}_i} \nabla W_{\mu,j}(\boldsymbol{\xi}_i) = \mathbf{0}, \tag{5}$$

and

$$HW_{\mu,j}(\boldsymbol{\xi}_i) = \mathbf{0} \text{ for all } \boldsymbol{\xi}_i \notin \sigma_j, \quad \sum_{j \in \mathcal{J}_i} HW_{\mu,j}(\boldsymbol{\xi}_i) = \mathbf{0}, \tag{6}$$

where, as usual, $\nabla W_{\mu,j}(\boldsymbol{x})$ and $HW_{\mu,j}(\boldsymbol{x})$ denote the gradient and the hessian matrix of $W_{\mu,j}(\boldsymbol{x})$, respectively. Finally, they are rational functions without singularities if μ is an even integer (for more details, see [24]).

The MS operator is a blend of local interpolation polynomials realized by using multinode basis functions as follows

$$\mathcal{MS}_\mu[f](\boldsymbol{x}) = \sum_{j=1}^{s} W_{\mu,j}(\boldsymbol{x}) P_j(\boldsymbol{x}).$$

Since the property (3) $\mathcal{MS}_\mu[\cdot]$ reproduces polynomials of d variables of total degree $\leq r$, while (4) imply that $\mathcal{MS}_\mu[f]$ interpolates data f_i at $\boldsymbol{\xi}_i$, $i = 1, \dots, n$. Moreover, by taking into account that for each $j \in \mathcal{J}_i$ there exists a unique $\iota \in \{1, \dots, m\}$ such that $j_\iota = i$, with a little abuse of notation we denote the polynomial $\ell_{j,\iota}$ by $\ell_{j,i}$ and rewrite the MS operator as follows

$$\mathcal{MS}_\mu[f](\boldsymbol{x}) = \sum_{i=1}^{n} \sum_{j \in \mathcal{J}_i} W_{\mu,j}(\boldsymbol{x}) \ell_{j,i}(\boldsymbol{x}) f_i = \sum_{i=1}^{n} B_{\mu,i}(\boldsymbol{x}) f_i \tag{7}$$

where, for each $i = 1, \dots, n$ we set

$$B_{\mu,i}(\boldsymbol{x}) = \sum_{j \in \mathcal{J}_i} W_{\mu,j}(\boldsymbol{x}) \ell_{j,i}(\boldsymbol{x}). \tag{8}$$

Functions $B_{\mu,i}(\boldsymbol{x})$ are linearly independent on the set $\{\boldsymbol{\xi}_1, \dots, \boldsymbol{\xi}_n\}$ since they satisfy the Kronecker delta property

$$B_{\mu,i}(\boldsymbol{\xi}_k) = \delta_{ki}, \quad k, i = 1, \dots, n. \tag{9}$$

In the following, it is useful to split the sum over i in (7) in two parts, the first one related to the interior points of the integration domain Ω and the second one related to the boundary points of Ω. Moreover, without loss of generality, we can assume that the nodes in Ξ are ordered in such a way that $\boldsymbol{\xi}_1, \dots, \boldsymbol{\xi}_{n_I}$ are the interior points and $\boldsymbol{\xi}_{n_I+1}, \dots, \boldsymbol{\xi}_n$ are the boundary points. Therefore we have

$$\mathcal{MS}_\mu[f](\boldsymbol{x}) = \sum_{i=1}^{n_I} B_{\mu,i}(\boldsymbol{x}) f_i + \sum_{i=n_I+1}^{n} B_{\mu,i}(\boldsymbol{x}) f_i. \tag{10}$$

3. Poisson problem with Dirichlet boundary conditions

In this section, we focus on the Poisson problem with continuous (or piecewise continuous) Dirichlet boundary conditions

$$\begin{cases} \Delta u(\boldsymbol{x}) = f(\boldsymbol{x}), & \boldsymbol{x} \in \Omega, \\ u(\boldsymbol{x}) = g(\boldsymbol{x}), & \boldsymbol{x} \in \partial\Omega, \end{cases} \tag{11}$$

and we assume, for $\mu > 2$ even integer, that its approximate solution $\tilde{u}$ is represented by (10), that is

$$\tilde{u}(\boldsymbol{x}) = \sum_{i=1}^{n_I} B_{\mu,i}(\boldsymbol{x}) \tilde{u}_i + \sum_{i=n_I+1}^{n} B_{\mu,i}(\boldsymbol{x}) \tilde{u}_i, \tag{12}$$

where $\tilde{u}_i = \tilde{u}(\boldsymbol{\xi}_i)$, $i = 1, \dots, n$, are the unknown coefficients. To determine these coefficients, we impose differential and boundary conditions to the approximate solution $\tilde{u}$ on the interior nodes $\boldsymbol{\xi}_1, \dots, \boldsymbol{\xi}_{n_I}$ and boundary nodes $\boldsymbol{\xi}_{n_I+1}, \dots, \boldsymbol{\xi}_n$, respectively. that is

$$\begin{cases} \Delta\tilde{u}(\boldsymbol{\xi}_k) &= f(\boldsymbol{\xi}_k), & k = 1, \dots, n_I, \\ \tilde{u}(\boldsymbol{\xi}_k) &= g(\boldsymbol{\xi}_k), & k = n_I + 1, \dots, n. \end{cases} \tag{13}$$

By taking into account the representation of the candidate solution (12) we can write (13) in matrix form as follows

$$A\tilde{\mathbf{u}} = \mathbf{y} \tag{14}$$

where we set $A = [A_{ki}], k, i = 1, \dots, n$, $\tilde{\mathbf{u}} = [\tilde{u}_1, \dots, \tilde{u}_n]^T$, $\mathbf{y} = [y_1, \dots, y_n]^T$, with $y_k = f(\boldsymbol{\xi}_k), k = 1, \dots, n_I$ and $y_k = g(\boldsymbol{\xi}_k), k = n_I + 1, \dots, n$.

By the setting (8), by the properties (4)–(6) satisfied by the basis functions $W_{\mu,j}$ and the Kronecker delta property (2) of the fundamental Lagrange polynomials $\ell_{j,i}$, simple algebraic computations show that the entries of the collocation matrix are

$$\begin{aligned} A_{ki} &= \Delta B_{\mu,i}(\boldsymbol{x})|_{\boldsymbol{x}=\boldsymbol{\xi}_k} \\ &= \sum_{j\in J_i} \Delta\left(W_{\mu,j}(\boldsymbol{x})\ell_{j,i}(\boldsymbol{x})\right)\Big|_{\boldsymbol{x}=\boldsymbol{\xi}_k} \\ &= \sum_{j\in J_i}\left(W_{\mu,j}(\boldsymbol{\xi}_k)\Delta\ell_{j,i}(\boldsymbol{\xi}_k) + 2\nabla W_{\mu,j}(\boldsymbol{\xi}_k)\cdot\nabla\ell_{j,i}(\boldsymbol{\xi}_k)\right), \qquad k=1,\dots,n_I,\ i=1,\dots,n, \end{aligned}$$

$$A_{ki} = 0, \qquad k = n_I+1,\dots,n \quad i=1,\dots,n_I$$

and finally

$$A_{ki} = \delta_{ki}, \qquad k,i = n_I+1,\dots,n.$$

Consequently

$$\tilde{u}_k = g(\boldsymbol{\xi}_k), \quad k = n_I+1,\dots,n$$

and the linear system (14) reduces to order n_I with

$$A_{ki} = \Delta B_{\mu,i}(\boldsymbol{x})|_{\boldsymbol{x}=\boldsymbol{\xi}_k}, \quad k,i=1,\dots,n_I, \tag{15}$$

and

$$y_k = f(\boldsymbol{\xi}_k) - \sum_{i=n_I+1}^{n} \Delta B_{\mu,i}(\boldsymbol{x})|_{\boldsymbol{x}=\boldsymbol{\xi}_k} g(\boldsymbol{\xi}_i), \qquad k=1,\dots,n_I. \tag{16}$$

We emphasize that the unknown vector is now related only to the Laplacian of the functions $B_{\mu,i}(\boldsymbol{x})$, $i=1,\dots,n_I$ which are linearly independent on $\left\{\boldsymbol{\xi}_1,\dots,\boldsymbol{\xi}_{n_I}\right\}$ by (9). However, the non singularity of the matrix A for general configuration of collocation nodes $\left\{\boldsymbol{\xi}_1,\dots,\boldsymbol{\xi}_n\right\}$ is still an open problem.

As a consequence of the polynomial reproduction property of the operator $\mathcal{MS}_\mu$, the following result can be stated.

Theorem 3.1. *Let A be a non-singular matrix and assume that the problem (11) admits a unique polynomial solution $p\in\mathcal{P}_r(\mathbb{R}^d)$. Then $\tilde{u}=p$.*

Proof. By the polynomial reproduction property of the operator $\mathcal{MS}_\mu$ we have $\mathcal{MS}_\mu[p]=p$ and then $\Delta\mathcal{MS}_\mu[p]=\Delta p$. Being $\Delta f=\Delta p$ and $g=p$ in (11) the vector $\tilde{\mathbf{u}}=[p(\boldsymbol{\xi}_1),\dots,p(\boldsymbol{\xi}_n)]$ is the unique solution of system (14) and the thesis follows since, by (12)

$$\tilde{u}(\boldsymbol{x}) = \sum_{i=1}^{n_I} B_{\mu,i}(\boldsymbol{x})\,p(\boldsymbol{\xi}_i) + \sum_{i=n_I+1}^{n} B_{\mu,i}(\boldsymbol{x})\,p(\boldsymbol{\xi}_i) = p(\boldsymbol{x}). \qquad \blacksquare$$

Remark 3.2. Theorem 3.1 holds in the case of more general BVPs for elliptic PDEs, when a covering $\left\{C_1(\partial\Omega),\dots,C_t(\partial\Omega)\right\}$ of $\partial\Omega$ by its pairwise disjoint connected subsets and differential operators $\mathcal{L},\mathcal{L}_1,\dots,\mathcal{L}_t$ are given, such that problem

$$\begin{cases} \mathcal{L}u(\boldsymbol{x}) = f(\boldsymbol{x}), & \boldsymbol{x}\in\Omega, \\ \mathcal{L}_1 u(\boldsymbol{x}) = g_1(\boldsymbol{x}), & \boldsymbol{x}\in C_1(\partial\Omega), \\ \vdots & \vdots \\ \mathcal{L}_t u(\boldsymbol{x}) = g_t(\boldsymbol{x}), & \boldsymbol{x}\in C_t(\partial\Omega), \end{cases}$$

admits a unique polynomial solution $p\in\mathcal{P}_r(\mathbb{R}^d)$.

In the following, we assume $d=2$ and set $\boldsymbol{x}=(x,y)$. Moreover, we fix the value of μ to 4 in order to work with rational approximants satisfying both properties (5)–(6). In Algorithm 1 we report the pseudocode for the Multinode Shepard Collocation (MSC) method.

In the numerical experiments, provided in the following sections, we compare the results obtained by using the MSC method with those obtained by the Kansa method [6] with the following RBFs:

$$\begin{array}{ll} \text{Hardy's Multiquadric } C^\infty \text{ (MQ)} & \varphi(\rho) = \left(1+c^2\rho^2\right)^{\frac{1}{2}}; \\ \text{Inverse Multiquadric } C^\infty \text{ (IMQ)} & \varphi(\rho) = \left(1+c^2\rho^2\right)^{-\frac{1}{2}}; \\ \text{Matérn } C^6 \text{ (M6)} & \varphi(\rho) = e^{-c\rho}\left(15+15c\rho+6c^2\rho^2+c^3\rho^3\right), \end{array} \tag{17}$$

Table 1
Parameter values for the experiment in Fig. 2.

r	m	q	s
3	10	10	16
4	15	1	9
5	21	4	9
6	28	5	7
7	3	8	6
8	45	3	4
9	55	3	2

where $\rho = \|\boldsymbol{x}\| = \sqrt{x^2 + y^2}$ and $c > 0$ is the shape parameter, which plays an important role in the accuracy of the method and is set by means of trial and error procedure [25,26]. Moreover, we consider a comparison with the polynomial-augmented RBF Kansa method [10], by adding a polynomial term to get the same reproduction degree r as the MSC method.

Algorithm 1 Algorithm for the MSC method

Require: A set of collocation points $\Xi = \{\boldsymbol{\xi}_i\}_{i=1}^{n}$; r degree of the local polynomial interpolants; $m = \binom{r+2}{2}$; $m + q$, $q > 0$, number of nearest neighbor points for the selection of the covering $\{\sigma_j\}_{j=1}^{s}$
Ensure: Approximation of the solution $u(\boldsymbol{x})$
`Step 1:` Determine the minimal set $\{\sigma_j\}_{j=1}^{s}$ covering Ξ
`Step 2:` Compute the entries of the collocation matrix by the formula (15)
`Step 3:` Compute the entries of the known term by the formula (16)
`Step 4:` Solve the linear system $A\tilde{\boldsymbol{u}} = \boldsymbol{y}$ to compute the approximation $\tilde{\boldsymbol{u}}_i$ of the solution $u(\boldsymbol{x})$ at the collocation points $\boldsymbol{\xi}_i$, $i = 1, \dots, n_I$
`Step 5:` Reconstruct the approximation of $u(\boldsymbol{x})$ through the MS approximant in (12)

3.1. Elliptic problems on the unit disk with Dirichlet boundary conditions

We focus on the elliptic problem (11), with $\Omega = \{(x, y) \in \mathbb{R}^2 : x^2 + y^2 \leq 1\}$ being the unit disk centered at the origin, and

$$u(x, y) = \frac{65}{65 + (x - 0.2)^2 + (y + 0.1)^2}.$$

This problem has been approached in [13], in order to study the conditioning of the collocation matrix, when the shape parameter c tends to 0, by means of three slightly different variations of the Kansa pure collocation method. For the aim of the paper [13], a small number of collocation points is sufficient. In our experiment, we consider the set of 50 Halton points in $[0, 1] \times [0, 1]$, moved into $[-1, 1] \times [-1, 1]$ by means of the affine map

$$\boldsymbol{x} \mapsto 2\left(\boldsymbol{x} - \frac{1}{2}\right), \qquad \boldsymbol{x} = (x, y) \in \mathbb{R}^2,$$

from which we extract the subset of points that lie in the unit disk Ω. As a result, we get $n_I = 41$ interior points which we couple with $n_B = 22$ uniformly distributed boundary points (see Fig. 1 (left)). We compute the mean absolute error and the condition number of the collocation matrix obtained by using the Kansa method and the polynomial-augmented Kansa method with RBFs in (17) with the best shape parameters ($c = 0.11$ for the MQ, $c = 0.21$ for the IMQ and $c = 0.31$ for the M6) and the MSC method varying the degree r of the local polynomial interpolants from 3 to 9. We stress that the polynomial term in the polynomial-augmented Kansa method is chosen to get the same reproduction degree as the MSC method for each r. The shape parameter c used in the simulations is chosen using a trial and error procedure. The minimum degree $r = 3$ of the polynomial interpolants is necessary to avoid local interpolants with constant Laplacian. In its turn, the maximum degree $r = 9$ is determined by the total number of collocation points, which does not allow the use of local polynomial interpolants of greater degree. The pointwise errors are computed at a set of 801 points distributed on concentric circles of radii $i/8$, $i = 0, \dots, 8$ (see Fig. 1 (right)). The numerical results are displayed in Fig. 2. For each value of r, the covering $\{\sigma_j\}_{j=1}^{s}$ satisfying condition (1) is realized by minimizing the number s of subsets. The values of q and s are reported in Table 1. As one expects, by increasing the degree of the local polynomial interpolants, and therefore the polynomial reproduction degree of the approximate solution (12), the accuracy of the MSC method increases. In particular, the numerical results, summarized in Fig. 2 and in Fig. 3, show an improvement in the accuracy of the approximation of the MSC method from a value of $2.63e{-}5$ for $r = 3$ up to a value of $7.44e{-}12$ for $r = 9$ and a low condition number which does not vary as the polynomial degree increases.

Finally, in Fig. 4 we plot the error on the surface of the approximate solutions obtained by the MSC method with $r = 9$, the Kansa M6 method, and the polynomial-augmented Kansa IMQ method with $r = 9$ by using $n = 63$ collocation points.

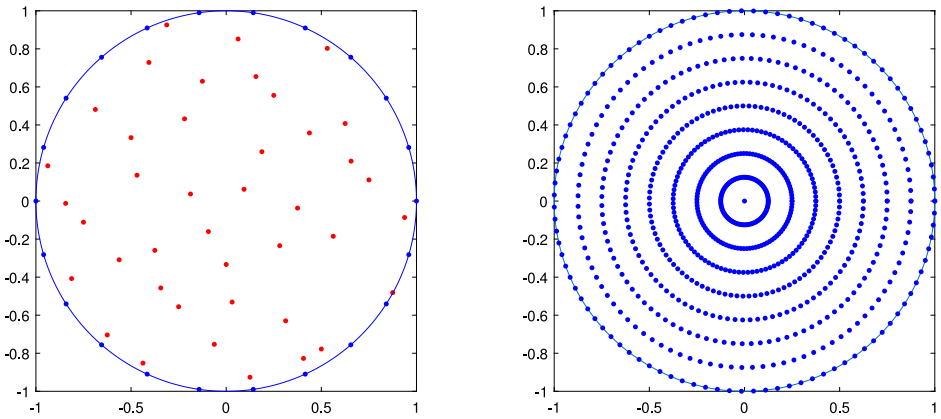

Fig. 1. Point distributions for the example in Section 3.1. Left: the set of $n_I = 41$ Halton interior points in red with $n_B = 22$ uniformly distributed boundary points in blue. Right: the set of 801 evaluation points arranged on concentric circles of radii $i/8$, $i = 0, \ldots, 8$.

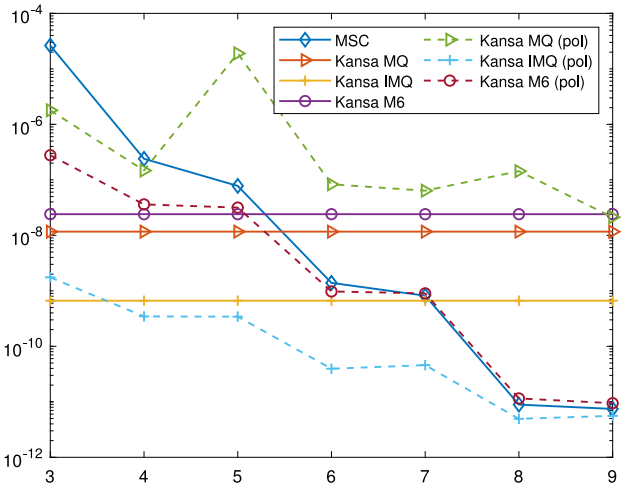

Fig. 2. Semilog plots of the mean absolute error for the example presented in Section 3.1. The MSC method is with r from 3 to 9. The same values of r are for the polynomial-augmented Kansa method (pol). The shape parameter for the RBFs in (17) are $c = 0.11$ for the MQ, $c = 0.21$ for the IMQ and $c = 0.31$ for the M6.

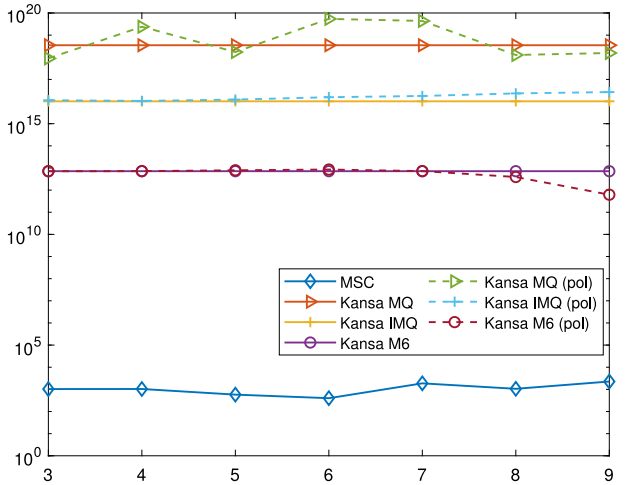

Fig. 3. Semilog plots of the condition number of the collocation matrices for the example presented in Section 3.1. The MSC method is with r from 3 to 9. The same values of r are for the polynomial-augmented Kansa method (pol). The shape parameter for the RBFs in (17) are $c = 0.11$ for the MQ, $c = 0.21$ for the IMQ and $c = 0.31$ for the M6.

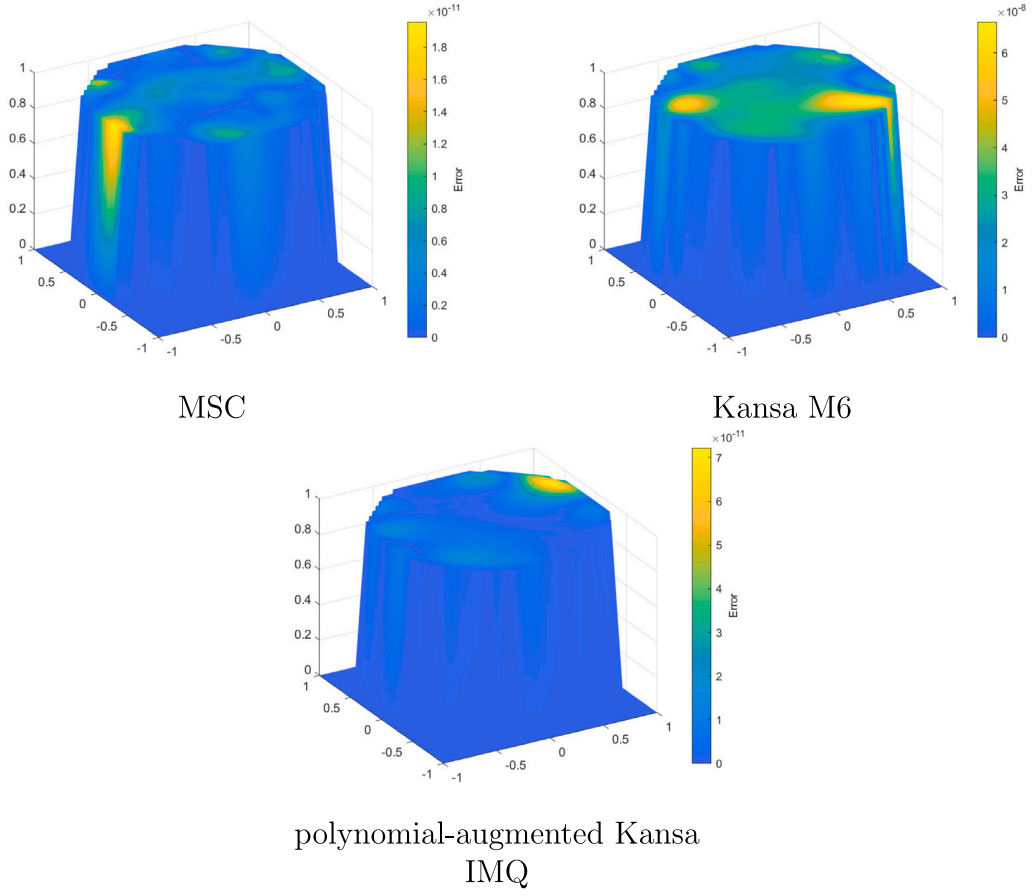

Fig. 4. Error on the surface of the approximated solution for the example presented in Section 3.1. The MSC method, on the top left, is with $r = 9$. The Kansa M6 method is on the top right and the polynomial-augmented Kansa IMQ method, on the bottom, is with $r = 9$. The simulations use $n_I = 41$ Halton interior points and $n_B = 22$ uniformly distributed boundary points.

3.2. Elliptic problem on L-shaped domain with Dirichlet boundary conditions

Let us consider the L-shaped domain

$$\bar{\Omega} = [0, 0.5] \times [0, 1] \cup [0.5, 1] \times [0, 0.5]$$

and the function [27]

$$u(x, y) = \sin(\pi x) \cos\left(\frac{\pi y}{2}\right)$$

solution, on $\bar{\Omega}$, of the corresponding Poisson problem with Dirichlet boundary conditions (11). To test how the MSC method performs in numerically solving this problem, we consider the set of 500 Halton points in $[0, 1] \times [0, 1]$ from which we extract the maximal subset of points that lie in the L-shaped domain Ω. As a result, we get a set of $n_I = 376$ interior points which we couple with $n_B = 82$ uniformly distributed boundary points, respectively (see Fig. 5). Moreover, the local polynomial interpolant degree r varies from 4 to 11. For each value of r, the covering $\{\sigma_j\}_{j=1}^{s}$ satisfying condition (1) is realized by minimizing the number s of subsets. The values of q and s are reported in Table 2. The Kansa method and the polynomial-augmented Kansa method adopt the best shape parameters for the employed RBFs ($c = 1.9$ for the MQ, $c = 1.8$ for the IMQ and $c = 0.8$ for the M6). The shape parameters c used in the simulations are chosen using a trial and error procedure. We stress that the polynomial term in the polynomial-augmented Kansa method is chosen to get the same polynomial reproduction degree as the MSC method for each r. The pointwise errors are evaluated at a set of 7500 points distributed on a regular grid on the L-shaped domain and the mean absolute error and the condition number of the collocation matrices are computed for overall methods. The numerical results are displayed in Fig. 6. In Fig. 7 we represent the error on the surface of the approximate solution for the case $r = 11$. Finally, in Fig. 8 we display the semilog plot of the condition number of the various collocation matrices by varying the polynomial reproduction degree r.

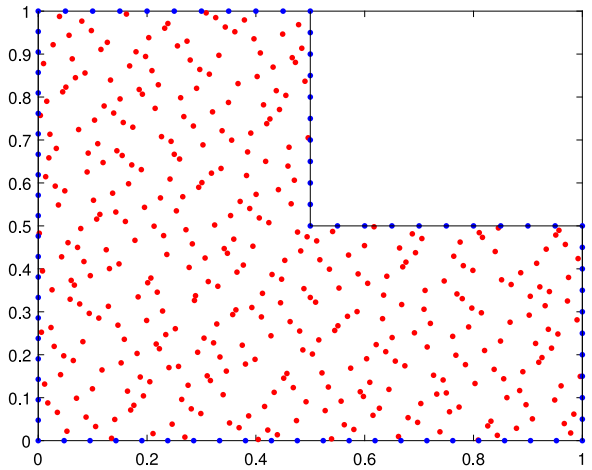

Fig. 5. L-shaped domain, for the example in Section 3.2, with the set of interior Halton points in red and uniformly distributed boundary points in blue.

Table 2
Parameter values for the experiment in Fig. 6.

r	m	q	s
4	15	10	87
5	21	14	70
6	28	9	52
7	36	13	44
8	45	4	32
9	55	9	29
10	66	15	29
11	78	18	24

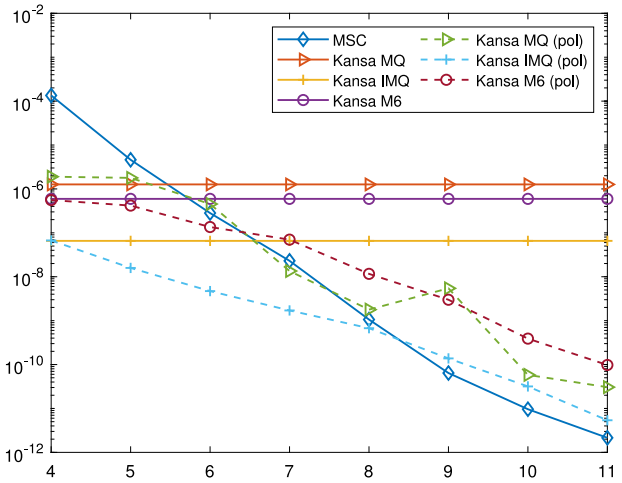

Fig. 6. Semilog plots of the mean absolute error for the example presented in Section 3.2. The MSC method is with r from 4 to 11. The same values of r are for the polynomial-augmented Kansa method (pol). The shape parameter for the RBFs in (17) are $c = 1.8$ for the MQ, $c = 1.9$ for the IMQ and $c = 1.4$ for the M6.

4. Seepage flow in a heterogeneous and anisotropic medium

In hydrology, seepage flow refers to the flow of a fluid (water) in permeable soil layers such as sand. From the mathematical point of view, such a problem is formulated by a PDE problem based on an extension of Darcy's law [28]. More precisely, the mathematical

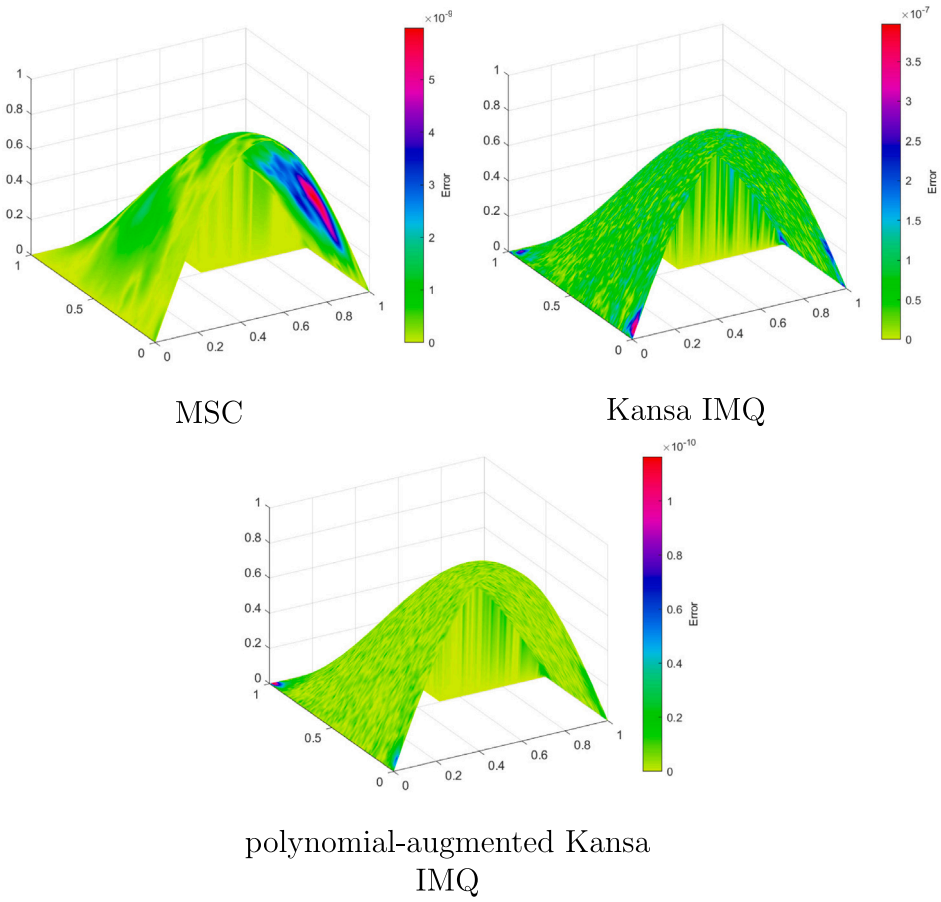

Fig. 7. Error on the surface of the approximated solution for the example presented in Section 3.2. The MSC method, on the top left, is with $r = 11$. The Kansa IMQ method with $c = 1.8$ is on the top right and the polynomial-augmented Kansa IMQ method, on the bottom, is with $c = 1.8$ and $r = 11$. The simulations use $n_I = 376$ interior points and $n_B = 82$ uniformly distributed boundary points.

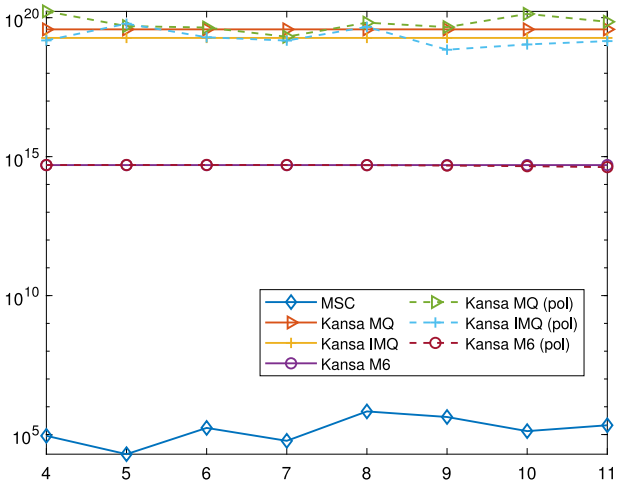

Fig. 8. Semilog plots of the condition number of the collocation matrices for the example presented in Section 3.2. The MSC method is with r from 4 to 11. The same values of r are for the polynomial-augmented Kansa method (pol). The shape parameter for the RBFs in (17) are $c = 1.8$ for both RBF methods.

model for the seepage flow in a heterogeneous and anisotropic medium corresponds to an elliptic operator with variable coefficients coupled with Dirichlet boundary conditions

$$\begin{cases} \dfrac{\partial}{\partial x}\left[a(x,y)\dfrac{\partial u}{\partial x}\right]+\dfrac{\partial}{\partial y}\left[b(x,y)\dfrac{\partial u}{\partial y}\right]=f(x,y), & (x,y)\in\Omega,\\ u(x,y)=g(x,y), & (x,y)\in\partial\Omega, \end{cases} \tag{18}$$

where the derivatives

$$v(x,y)=-a(x,y)\frac{\partial u}{\partial x},\qquad w(x,y)=-b(x,y)\frac{\partial u}{\partial y},$$

represent the Darcy's velocity [27]. If $a(x,y)=b(x,y)=k$, $k\in\mathbb{R}\setminus\{0\}$, the problem (18) becomes a Poisson problem with Dirichlet boundary conditions. In applying the MSC method to approximate the solution u of the problem (18), as before we distinguish between interior and boundary collocation points. By the setting (8), by the properties (4)–(6) satisfied by the basis functions $W_{\mu,j}$ and the Kronecker delta property (2) of the fundamental Lagrange polynomials $\ell_{j,i}$, simple algebraic computations show that the entries of the collocation matrix are

$$\begin{aligned} A_{ki} &= \left(\frac{\partial}{\partial x}\left[a(\boldsymbol{x})\frac{\partial B_{\mu,i}}{\partial x}(\boldsymbol{x})\right]+\frac{\partial}{\partial y}\left[b(\boldsymbol{x})\frac{\partial B_{\mu,i}}{\partial y}(\boldsymbol{x})\right]\right)\Bigg|_{\boldsymbol{x}=\boldsymbol{\xi}_k} \qquad k=1,\dots,n_I,\ i=1,\dots,n,\\ &= \frac{\partial a}{\partial x}(\boldsymbol{\xi}_k)\sum_{j\in\mathcal{J}_i}W_{\mu,j}(\boldsymbol{\xi}_k)\frac{\partial \ell_{j,i}}{\partial x}(\boldsymbol{\xi}_k)+a(\boldsymbol{\xi}_k)\sum_{j\in\mathcal{J}_i}\left(\frac{\partial W_{\mu,j}}{\partial x}(\boldsymbol{\xi}_k)\frac{\partial \ell_{j,i}}{\partial x}(\boldsymbol{\xi}_k)+W_{\mu,j}(\boldsymbol{\xi}_k)\frac{\partial^2 \ell_{j,i}}{\partial x^2}(\boldsymbol{\xi}_k)\right)\\ &\quad+\frac{\partial b}{\partial y}(\boldsymbol{\xi}_k)\sum_{j\in\mathcal{J}_i}W_{\mu,j}(\boldsymbol{\xi}_k)\frac{\partial \ell_{j,i}}{\partial y}(\boldsymbol{\xi}_k)+b(\boldsymbol{\xi}_k)\sum_{j\in\mathcal{J}_i}\left(\frac{\partial W_{\mu,j}}{\partial y}(\boldsymbol{\xi}_k)\frac{\partial \ell_{j,i}}{\partial y}(\boldsymbol{\xi}_k)+W_{\mu,j}(\boldsymbol{\xi}_k)\frac{\partial^2 \ell_{j,i}}{\partial y^2}(\boldsymbol{\xi}_k)\right),\\ A_{ki}&=0,\qquad k=n_I+1,\dots,n,\qquad i=1,\dots,n_I \end{aligned}$$

and finally

$$A_{ki}=\delta_{ki},\qquad k,i=n_I+1,\dots,n.$$

Consequently

$$\tilde{u}_k=g(\boldsymbol{\xi}_k),\quad k=n_I+1,\dots,n$$

and the collocation linear system reduces to order n_I with

$$A_{ki}=\left(\frac{\partial}{\partial x}\left[a(\boldsymbol{x})\frac{\partial B_{\mu,i}}{\partial x}(\boldsymbol{x})\right]+\frac{\partial}{\partial y}\left[b(\boldsymbol{x})\frac{\partial B_{\mu,i}}{\partial y}(\boldsymbol{x})\right]\right)\Bigg|_{\boldsymbol{x}=\boldsymbol{\xi}_k},\quad k,i=1,\dots,n_I,$$

and

$$y_k=f(\boldsymbol{\xi}_k)-\sum_{i=n_I+1}^{n}\left(\frac{\partial}{\partial x}\left[a(\boldsymbol{x})\frac{\partial B_{\mu,i}}{\partial x}(\boldsymbol{x})\right]+\frac{\partial}{\partial y}\left[b(\boldsymbol{x})\frac{\partial B_{\mu,i}}{\partial y}(\boldsymbol{x})\right]\right)\Bigg|_{\boldsymbol{x}=\boldsymbol{\xi}_k} g(\boldsymbol{\xi}_i),\qquad k=1,\dots,n_I.$$

4.1. A case study

In line with [27], we set

$$a(x,y)=2-x^2-y^2,\qquad b(x,y)=e^{x-y},$$

and, on $\bar{\Omega}=[0,1]\times[0,1]$, we consider the function

$$u(x,y)=xy(1-x)(1-y),$$

solution of the corresponding seepage flow problem (18) with

$$f(x,y)=-xe^{x-y}(1-x)(3-2y)+2y(1-y)(3x^2+y^2-x-2).$$

In line with [27], we conduct the experiments by using $n_I=113$ interior points and $n_B=32$ boundary points. In Fig. 9 we display the error on the surface of the approximated solution obtained by the MSC method with local interpolation polynomial of degree $r=4$ and those obtained by using the Kansa MQ method with shape parameter $c=1.2$ and the polynomial-augmented Kansa MQ method with $r=4$ and shape parameter $c=1.2$. The error is computed on a regular grid of 100×100 points on the solution domain $\bar{\Omega}$. The covering $\{\sigma_j\}_{j=1}^{s}$ satisfying condition (1) is realized by minimizing the number s of subsets. By setting $m=15$ and $q=6$ we get $s=30$ subsets. Since the solution is a polynomial of degree 3, from Theorem 3.1 we expect $\tilde{u}=u$ and the obtained numerical results related to the absolute error of $6.03e{-}16$ for the MSC method confirm the thesis of the Theorem (see Fig. 9). By applying the Kansa MQ method we get a maximum absolute error of $2.24e{-}5$ while the polynomial-augmented Kansa MQ method gives a maximum absolute error of $9.07e{-}16$.

Moreover, the condition number of the MSC method is $1.60e{+}3$ against a condition number of $8.12e{+}13$ for the Kansa MQ method and of $7.80e{+}13$ for the polynomial-augmented Kansa MQ.

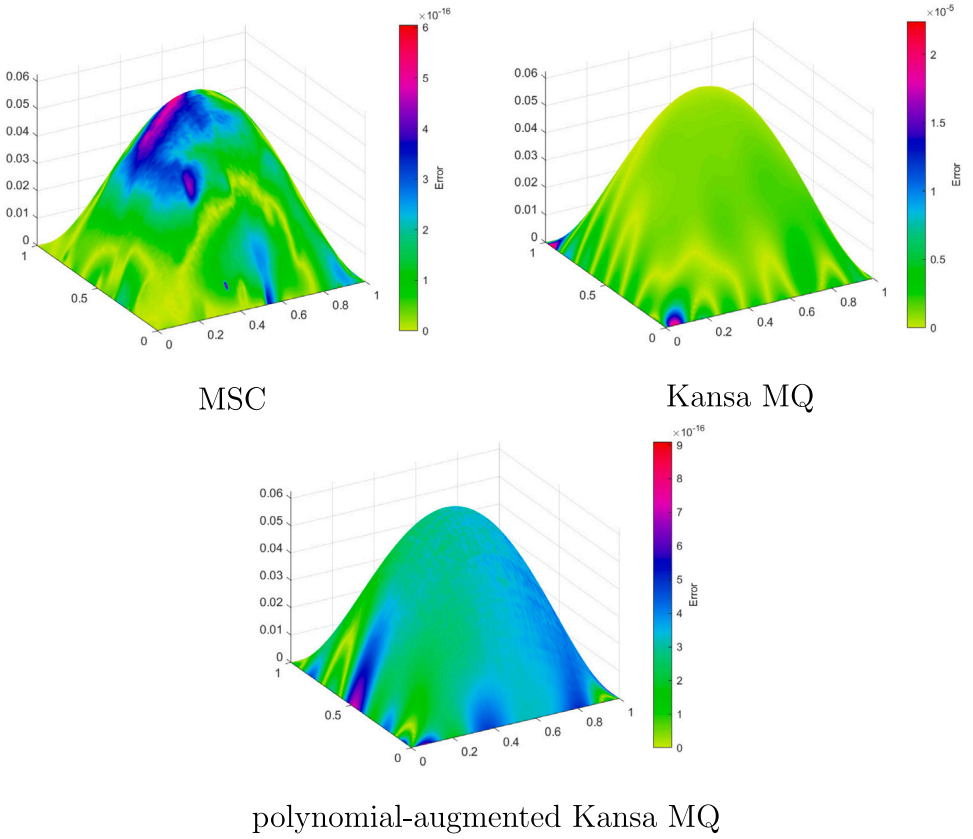

Fig. 9. Error on the surface of the approximated solution for the example presented in Section 4.1. The MSC method, on the top left, is with $r = 4$. The Kansa MQ method with $c = 1.2$ is on the top right and the polynomial-augmented Kansa MQ method, on the bottom, is with $c = 1.2$ and $r = 4$. The simulations use $n_I = 113$ interior points and $n_B = 32$ uniformly distributed boundary points.

5. Poisson problem with mixed boundary conditions

In this Section, we consider the Poisson problem with mixed boundary conditions on different shaped domains. In particular, we analyze the case in which the boundary conditions are constituted by both Dirichlet and Neumann conditions. Due to the particular nature of such problems, the entries of the collocation matrix depend on the Neumann conditions of the specific problem and therefore we cannot give a general representation for it as we do for the case of Dirichlet boundary conditions.

5.1. Poisson problem with mixed boundary conditions on the unit square domain

Let $\bar{\Omega}$ be the unit square $[0,1]\times[0,1]$. In line with [5], we consider the Poisson problem

$$\Delta u(x,y) = -5.4x \text{ in } \Omega \tag{19}$$

with the mixed Dirichlet–Neumann conditions

$$\begin{cases} \dfrac{\partial}{\partial y}u(x,y) = 0, & y = 0, \quad 0 \le x \le 1, \quad \Gamma_1, \\ u(x,y) = 0.1, & x = 1, \quad 0 \le y \le 1, \quad \Gamma_2, \\ -\dfrac{\partial}{\partial y}u(x,y) = 0, & y = 1, \quad 0 \le x < 1 \quad \Gamma_3, \\ u(x,y) = 1, & x = 0, \quad 0 \le y \le 1, \quad \Gamma_4, \end{cases} \tag{20}$$

whose exact solution is the cubic polynomial

$$u(x,y) = 1 - 0.9x^3.$$

In Fig. 10 we display the geometry domain of this problem. In applying the MSC method to approximate the solution u of the problem (19) with boundary conditions (20), we have to distinguish between interior and boundary collocation points. Without loss of generality, we assume that the collocation points are ordered as follows:

$$\begin{aligned}
&\xi_k \in \Omega, && k = 1, \dots, n_I;\\
&\xi_k \in \Gamma_1 \cup \Gamma_3, && k = n_I + 1, \dots, n_I + n_{BN};\\
&\xi_k \in \Gamma_2 \cup \Gamma_4, && k = n_I + n_{BN} + 1, \dots, n;
\end{aligned}$$

where n_{BN} is the number of collocation points on $\Gamma_1 \cup \Gamma_3$. By the setting (8), by the properties (4)–(6) satisfied by the basis functions $W_{\mu,j}$ and the Kronecker delta property (2) of the fundamental Lagrange polynomials $\ell_{j,i}$, simple algebraic computations show that the entries of the collocation matrix are

$$\begin{aligned}
A_{ki} &= \Delta B_{\mu,i}(\boldsymbol{x})|_{\boldsymbol{x}=\xi_k}\\
&= \sum_{j\in J_i} \Delta\left(W_{\mu,j}(\boldsymbol{x})\,\ell_{j,i}(\boldsymbol{x})\right)\Big|_{\boldsymbol{x}=\xi_k}\\
&= \sum_{j\in J_i} \left(W_{\mu,j}(\xi_k)\,\Delta\ell_{j,i}(\xi_k) + 2\nabla W_{\mu,j}(\xi_k)\cdot\nabla\ell_{j,i}(\xi_k)\right), \qquad k = 1,\dots,n_I,\ i = 1,\dots,n,
\end{aligned}$$

$$\begin{aligned}
A_{ki} &= \frac{\partial B_{\mu,i}}{\partial y}(\xi_k)\\
&= \sum_{j\in J_i} W_{\mu,j}(\xi_k)\,\frac{\partial \ell_{j,i}}{\partial y}(\xi_k), \qquad k = n_I + 1,\dots,n_I + n_{BN},\ i = 1,\dots,n,
\end{aligned}$$

$$A_{ki} = 0, \qquad k = n_I + n_{BN} + 1,\dots,n, \qquad i = 1,\dots,n_I + n_{BN} + 1,$$

and finally

$$A_{ki} = \delta_{ki}, \qquad k, i = n_I + n_{BN} + 2,\dots,n.$$

By taking into account the Dirichlet boundary conditions (20) on Γ_2 and Γ_3, we get

$$\tilde{u}_k = u(\xi_k), \quad k = n_I + n_{BN} + 1,\dots,n,$$

and the collocation linear system reduces to order $n_I + n_{BN}$ with

$$\begin{aligned}
&A_{ki} = \Delta B_{\mu,i}(\boldsymbol{x})|_{\boldsymbol{x}=\xi_k}, && k = 1,\dots,n_I, && i = 1,\dots,n_I + n_{BN},\\
&A_{ki} = \frac{\partial B_{\mu,i}}{\partial y}(\xi_k), && k = n_I + 1,\dots,n_I + n_{BN}, && i = 1,\dots,n_I + n_{BN},
\end{aligned}$$

and

$$\begin{aligned}
&y_k = -5.4\xi_k^x - \sum_{i=n_I+n_{BN}+1}^{n} \Delta B_{\mu,i}(\boldsymbol{x})|_{\boldsymbol{x}=\xi_k}\, u(\xi_i), && k = 1,\dots,n_I,\\
&y_k = -\sum_{i=n_I+n_{BN}+1}^{n} \frac{\partial B_{\mu,i}}{\partial y}(\xi_k)\, u(\xi_i) && k = n_I + 1,\dots,n_I + n_{BN},
\end{aligned}$$

where we assume $\xi_k = (\xi_k^x, \xi_k^y)$. In line with [5], we conduct the experiments by using $n_I = 289$ Halton points as interior nodes and $n_B = 64$ uniformly distributed boundary points. In Table 3 we report the maximum absolute error e_{max}, the mean absolute error e_{mean} and the root mean square error e_{RMS} evaluated at a grid of 40×40 points in $[0,1]\times[0,1]$ obtained by the MSC method with local interpolation polynomial of degree $r = 4$, by the Kansa MQ method with $c = 1.1$, the Kansa IMQ and M6 methods with $c = 1.2$ and by the polynomial-augmented Kansa method with the same shape parameter and $r = 4$. The covering $\{\sigma_j\}_{j=1}^{s}$ satisfying conditions (1) is realized by minimizing the number s of subsets. By setting $m = 15$ and $q = 19$ we get $s = 69$ subsets. Since the solution is a polynomial of degree 3, from Theorem 3.1 we expect $\tilde{u} = u$ and the obtained numerical results related to the maximum absolute error of $9.57e{-}14$ for the MSC method confirm the thesis of the Theorem (see Fig. 11). In Table 4 we report the condition number of the methods adopted in the simulations. We note that the MSC method gives rise to a collocation matrix with the lowest condition number.

5.2. Poisson problem with mixed boundary conditions on an elliptical domain

Let us consider the elliptical domain

$$\bar{\Omega} = \left\{(x,y) \in \mathbb{R}^2 : \frac{x^2}{a^2} + \frac{y^2}{b^2} \le 1\right\}$$

with major and minor semiaxes a and b and, on it, the function [29,30]

$$u(x,y) = -\left(\frac{a^2b^2}{a^2+b^2}\right)\left(\frac{x^2}{a^2} + \frac{y^2}{b^2} - 1\right),$$

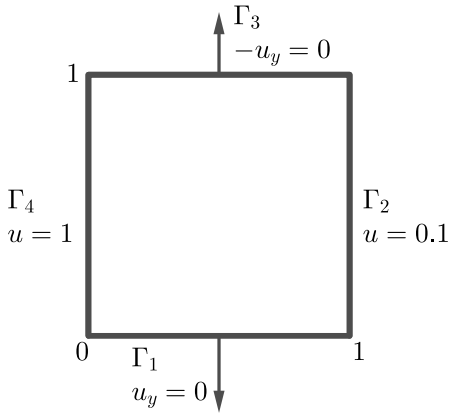

Fig. 10. The geometry domain of the problem in Section 5.1.

Table 3
Maximum absolute error e_{max}, mean absolute error e_{mean} and root mean square error e_{RMS} for the example presented in Section 5.1. The MSC method and the polynomial-augmented Kansa methods (pol) are with $r = 4$, $c = 1.2$ for the Kansa's IMQ, M6, polynomial-augmented IMQ and M6 methods, while $c = 1.1$ for the Kansa's MQ and polynomial-augmented MQ methods.

	e_{max}	e_{mean}	e_{RMS}
MSC	9.57e−14	2.70e−14	3.53e−14
Kansa MQ	3.19e−06	6.33e−07	7.91e−07
Kansa IMQ	2.51e−06	4.60e−07	5.96e−07
Kansa M6	6.57e−05	2.31e−06	5.27e−06
Kansa MQ (pol)	9.08e−11	2.68e−11	3.23e−11
Kansa IMQ (pol)	1.84e−09	5.98e−10	7.10e−10
Kansa M6 (pol)	3.53e−13	7.53e−14	1.06e−13

Table 4
Condition number for the example presented in Section 5.1. The MSC method and the polynomial-augmented Kansa methods (pol) are with $r = 4$, $c = 1.2$ for the Kansa's IMQ, M6, polynomial-augmented IMQ and M6 methods, while $c = 1.1$ for the Kansa's MQ and polynomial-augmented MQ methods.

	Condition number
MSC	6.41e+05
Kansa MQ	1.55e+19
Kansa IMQ	2.28e+19
Kansa M6	1.11e+14
Kansa MQ (pol)	5.16e+21
Kansa IMQ (pol)	1.47e+19
Kansa M6 (pol)	1.09e+14

solution of the Poisson problem with mixed boundary conditions

$$\begin{cases} \Delta u(\boldsymbol{x}) = -2, & \boldsymbol{x} \in \Omega, \\ \dfrac{\partial u}{\partial x} = 0, & x = 0, \\ \dfrac{\partial u}{\partial y} = 0, & y = 0, \\ u(\boldsymbol{x}) = 0, & \boldsymbol{x} \in \partial\Omega \setminus (0, y) \cup (x, 0)\,. \end{cases} \tag{21}$$

As specified in [31], the problem (21) provides a function u from which the angle of twist of a cylindrical shaft of an elliptical cross-section under torsion can be calculated. Moreover, since the solution of (21) is expected to be symmetric with respect to x and y, it is sufficient to solve it in the first quadrant of the ellipse. To this aim, in the experiments we consider the set of 100 Halton points in $[0, 1] \times [0, 1]$, moved into $[0, a] \times [0, a]$ by means of the affine map

$$\boldsymbol{x} \mapsto a\boldsymbol{x} \qquad \boldsymbol{x} = (x, y) \in \mathbb{R}^2,$$

from which we extract the subset of points that lie in the first quadrant of the ellipse of semiaxes a and b. The collocation matrix can be obtained similarly to the one discussed in Section 5.1. By following [29], in the first experiment we set $a = 10$, $b = 8$ and we get $n_I = 67$ interior points which we couple with $n_B = 44$ boundary points (see Fig. 12 (left)). We compute the maximum absolute error e_{max}, the mean absolute error e_{mean} and the root mean square error e_{RMS} by evaluating the pointwise errors at a set of 161

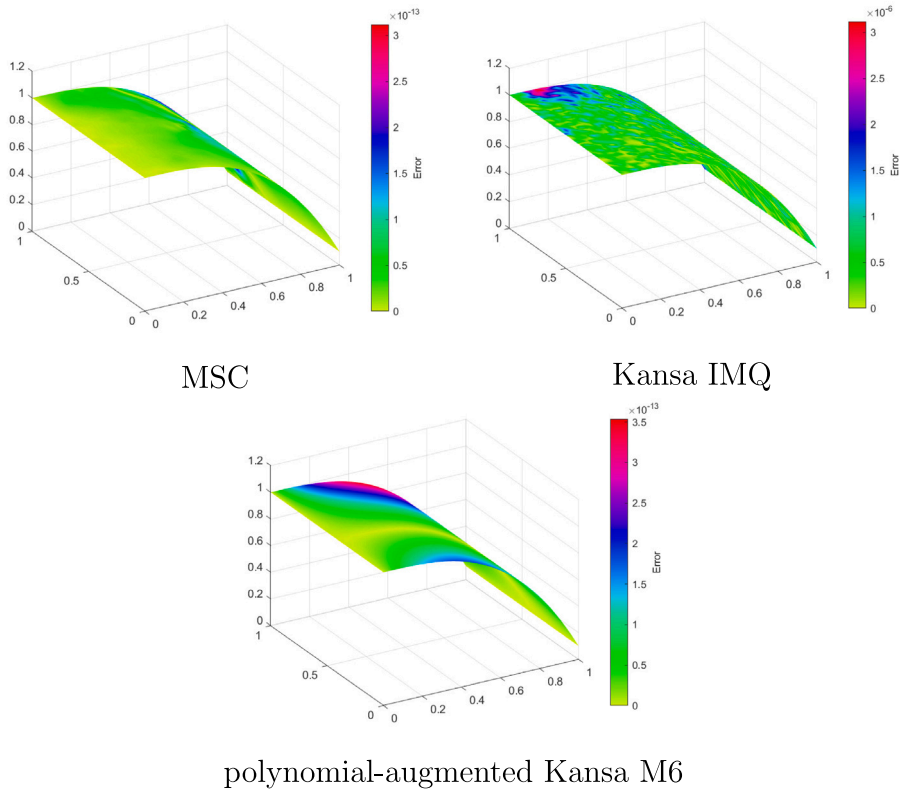

Fig. 11. Error on the surface of the approximated solution for the example presented in Section 5.1. The MSC method, on the top left, is with $r = 4$. The Kansa IMQ method with $c = 1.2$ is on the top right and the polynomial-augmented Kansa M6 method, on the bottom, is with $c = 1.2$ and $r = 4$. The simulations use $n_I = 289$ interior points and $n_B = 64$ uniformly distributed boundary points.

Table 5
Maximum absolute error e_{max}, mean absolute error e_{mean} and root mean square error e_{RMS} for the example presented in Section 5.2. The MSC method and the polynomial-augmented Kansa methods (pol) are with $r = 3$, $c = 0.1$ for the Kansa and polynomial-augmented Kansa methods. The collocation points lie in the first quadrant of the ellipse of semiaxes $a = 10$ and $b = 8$.

	e_{max}	e_{mean}	e_{RMS}
MSC	1.25e−12	1.59e−13	3.14e−13
Kansa MQ	1.49e−04	3.91e−05	6.83e−05
Kansa IMQ	1.03e−03	3.45e−04	5.49e−04
Kansa M6	3.94e−03	8.57e−04	1.66e−03
Kansa MQ (pol)	6.68e−08	3.28e−08	4.75e−08
Kansa IMQ (pol)	4.56e−10	2.29e−10	3.31e−10
Kansa M6 (pol)	6.31e−09	3.06e−09	4.52e−09

points in the first quadrant distributed on concentric ellipses of semiaxes $ai/16$ and $bi/16$, $i = 0, \dots, 16$ (see Fig. 12 (right)). The numerical results, obtained by the MSC method with local interpolation polynomials of degree $r = 3$, the Kansa method with the RBFs in (17) and the polynomial-augmented Kansa method with $r = 3$, are reported in Table 5. The best shape parameter is $c = 0.1$ for all the RBFs. The covering $\{\sigma_j\}_{j=1}^{s}$ satisfying condition (1) is realized by minimizing the number s of subsets. By setting $m = 10$ and $q = 10$ we get $s = 26$ subsets. In this case the values for the condition number are reported in Table 6, which shows again the best conditioning for the MSC method.

Finally, in Fig. 13 we display the error on the surface of the approximated solution obtained by the MSC method, the Kansa MQ method and the polynomial-augmented Kansa IMQ method. In the second experiment, we set $a = 2$ and $b = 1$ and we get $n_I = 40$ interior points which we couple with $n_B = 24$ boundary points. The related numerical results are reported in Table 7, where the best shape parameter for the Kansa MQ is $c = 0.3$, for the Kansa IMQ is $c = 0.2$ and for the Kansa M6 is $c = 0.1$.

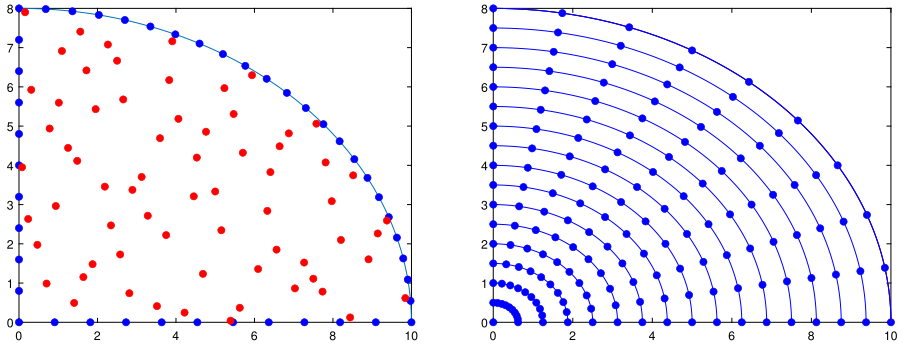

Fig. 12. Set of $n_I = 67$ Halton interior points in red with $n_B = 44$ boundary points in blue (left) and set of 161 evaluation points in the first quadrant distributed on concentric ellipses of semiaxes $10i/16$ and $8i/16$, $i = 0, \dots, 16$ used for the example presented in Section 5.2.

Table 6
Condition number for the example presented in Section 5.2. The MSC method and the polynomial-augmented Kansa methods (pol) are with $r = 4$, $c = 1.2$ for the Kansa's IMQ, M6, polynomial-augmented IMQ and M6 methods, while $c = 1.1$ for the Kansa's MQ and polynomial-augmented MQ methods.

	Condition number
MSC	2.16*e*+04
Kansa MQ	9.34*e*+17
Kansa IMQ	8.20*e*+17
Kansa M6	1.55*e*+13
Kansa MQ (pol)	1.55*e*+19
Kansa IMQ (pol)	1.35*e*+20
Kansa M6 (pol)	2.38*e*+17

Table 7
Maximum absolute error e_{max}, mean absolute error e_{mean} and root mean square error e_{RMS} for the example presented in Section 5.2. The MSC method and the polynomial-augmented Kansa methods (pol) are with $r = 3$, $c = 0.3$ for the Kansa MQ and polynomial-augmented MQ, $c = 0.2$ for the Kansa IMQ and polynomial-augmented IMQ and $c = 0.1$ for the Kansa M6 and polynomial-augmented M6. The collocation points lie in the first quadrant of the ellipse of semiaxes $a = 2$ and $b = 1$.

	e_{max}	e_{mean}	e_{RMS}
MSC	5.77*e*−15	2.85*e*−15	4.15*e*−15
Kansa MQ	1.90*e*−05	5.67*e*−06	9.44*e*−06
Kansa IMQ	1.53*e*−04	4.59*e*−05	7.16*e*−05
Kansa M6	3.70*e*−05	1.34*e*−05	2.07*e*−05
Kansa MQ (pol)	2.02*e*−11	1.32*e*−11	1.74*e*−11
Kansa IMQ (pol)	7.47*e*−11	4.85*e*−11	6.41*e*−11
Kansa M6 (pol)	2.30*e*−12	1.51*e*−12	2.01*e*−12

5.3. Poisson problem with mixed boundary conditions on the unit square domain with no polynomial exact solution

Let $\bar{\Omega} = [0,1] \times [0,1]$. In line with [30], we consider the Poisson problem

$$\Delta u(x,y) = (\lambda^2 + \nu^2) e^{\lambda x + \nu y}, \qquad (x,y) \in \Omega,$$

with the mixed Dirichlet–Neumann boundary conditions

$$\begin{cases} u(x,y) = e^{\lambda x + \nu y}, & y = 0, \quad 0 \le x \le 1, \\ u(x,y) = e^{\lambda x + \nu y}, & y = 1, \quad 0 \le x \le 1, \\ \dfrac{\partial u(x,y)}{\partial x} = \lambda e^{\lambda x + \nu y}, & x = 0, \quad 0 < y < 1, \\ \dfrac{\partial u(x,y)}{\partial x} = \lambda e^{\lambda x + \nu y}, & x = 1, \quad 0 < y < 1, \end{cases}$$

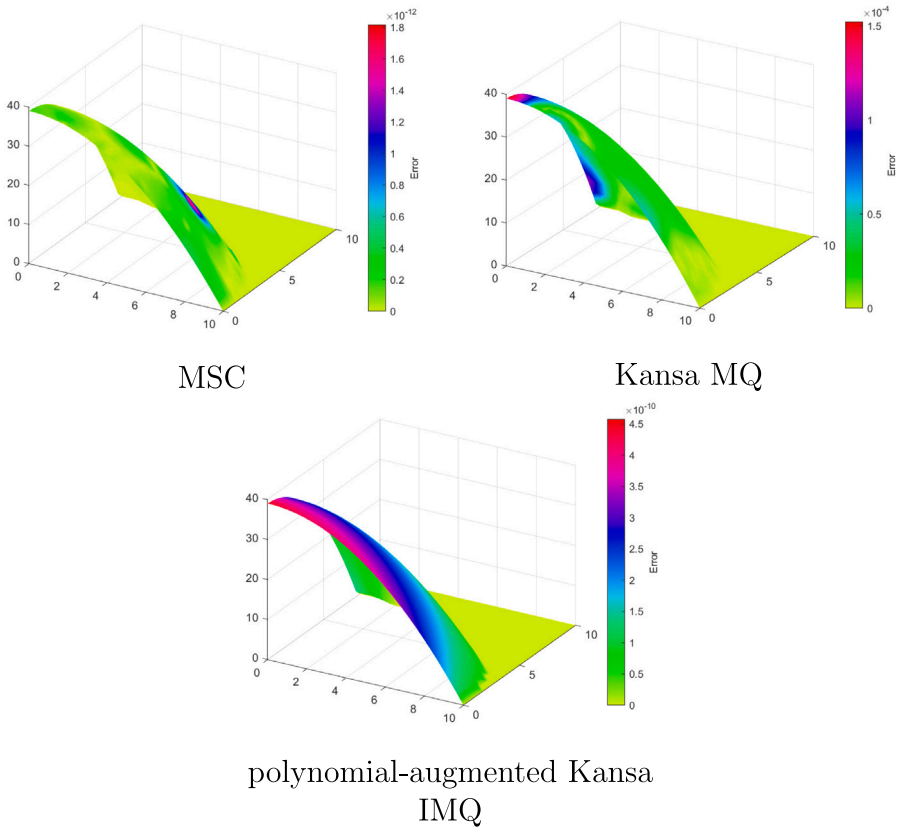

Fig. 13. Error on the surface of the approximated solution for the example presented in Section 5.2. The MSC method, on the top left, is with $r = 3$. The Kansa MQ method with $c = 0.1$ is on the top right and the polynomial-augmented Kansa IMQ method, on the bottom, is with $c = 0.1$ and $r = 3$. The simulations use $n_I = 67$ interior points and $n_B = 44$ uniformly distributed boundary points. The collocation points lie in the first quadrant of the ellipse of semiaxes $a = 10$ and $b = 8$.

whose exact solution is

$$u(x, y) = e^{\lambda x + \nu y}.$$

By following [6,30], we set $\lambda = 2$ and $\nu = 3$. In this case, the collocation matrix is the same as the one discussed in Section 5.1 with $\frac{\partial}{\partial x}$ in place of $\frac{\partial}{\partial y}$. To test how the MSC method performs in numerically solving this problem, we consider the set of $n_I = 500$ Halton points in $[0, 1] \times [0, 1]$ coupled with $n_B = 84$ uniformly distributed boundary points, respectively. Moreover, the local polynomial interpolant degree r varies from 4 to 11. For each value of r, the covering $\{\sigma_j\}_{j=1}^{s}$ satisfying condition (1) is realized by minimizing the number s of subsets. The values of q and s are reported in Table 8. The Kansa method and the polynomial-augmented Kansa method adopt the best shape parameters for the employed RBFs ($c = 2.1$ for the MQ, $c = 1.6$ for the IMQ and $c = 0.4$ for the M6). The shape parameters c used in the simulations are chosen using a trial and error procedure. We stress that the polynomial term in the polynomial-augmented Kansa method is chosen to get the same polynomial reproduction degree as the MSC method for each r. The pointwise errors are evaluated at a set of 40×40 points distributed on a regular grid on $[0, 1] \times [0, 1]$ and the mean absolute error and the condition number of the collocation matrices are computed for overall methods. The numerical results are displayed in Fig. 14. In Fig. 16 we represent the error on the surface of the approximated solution for the case $r = 11$. Finally, in Fig. 15 we display the semilog plot of the condition number of the various collocation matrices by varying the polynomial reproduction degree r.

6. Conclusion and future perspectives of work

In this paper, we investigated on the multinode Shepard method for solving elliptic boundary value problems equipped with Dirichlet and/or Neumann boundary conditions on two-dimensional domains of different shapes. The method performs very well by reaching good approximation accuracy comparable with or better than the one reached by the RBF Kansa methods with or without polynomial precision. We highlight the particular feature of the MSC method, which gives rise to a collocation matrix with a low condition number.

Table 8
Parameter values for the experiment in Fig. 14.

r	m	q	s
4	15	12	112
5	21	11	83
6	28	4	58
7	36	10	57
8	45	18	47
9	55	11	43
10	66	5	30
11	78	9	29

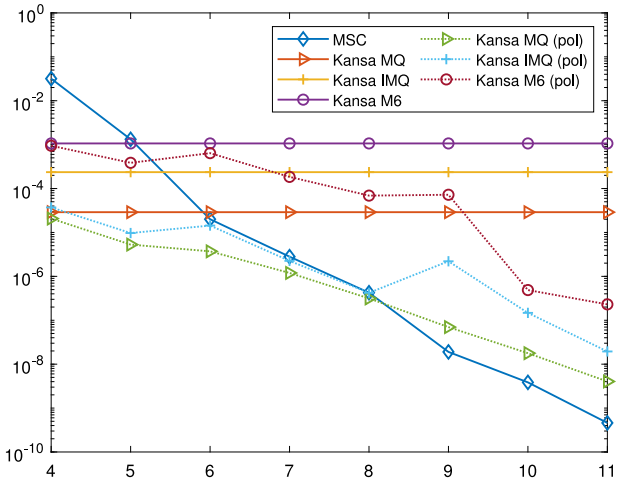

Fig. 14. Semilog plots of the mean absolute error for the example presented in Section 5.3. The MSC method is with r from 4 to 11. The same values of r are for the polynomial-augmented Kansa method (pol). The shape parameter for the RBFs in (17) are $c = 2.1$ for the MQ, $c = 1.6$ for the IMQ and $c = 0.4$ for the M6.

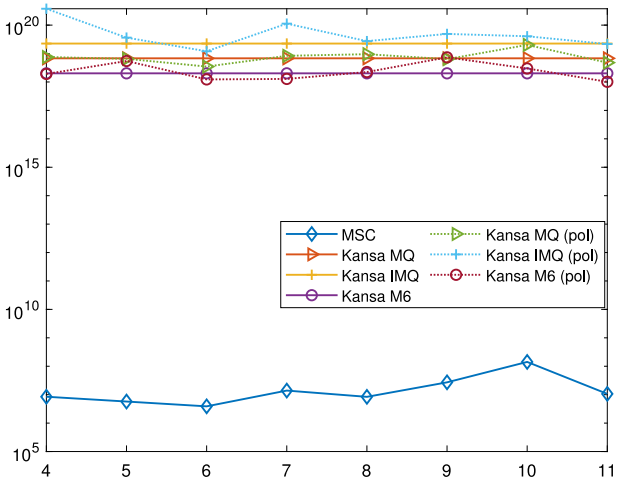

Fig. 15. Semilog plots of the condition number of the collocation matrices for the example presented in Section 5.3. The MSC method is with r from 4 to 11. The same values of r are for the polynomial-augmented Kansa method (pol). The shape parameter for the RBFs in (17) are $c = 2.1$ for the MQ, $c = 1.6$ for the IMQ and $c = 0.4$ for the M6.

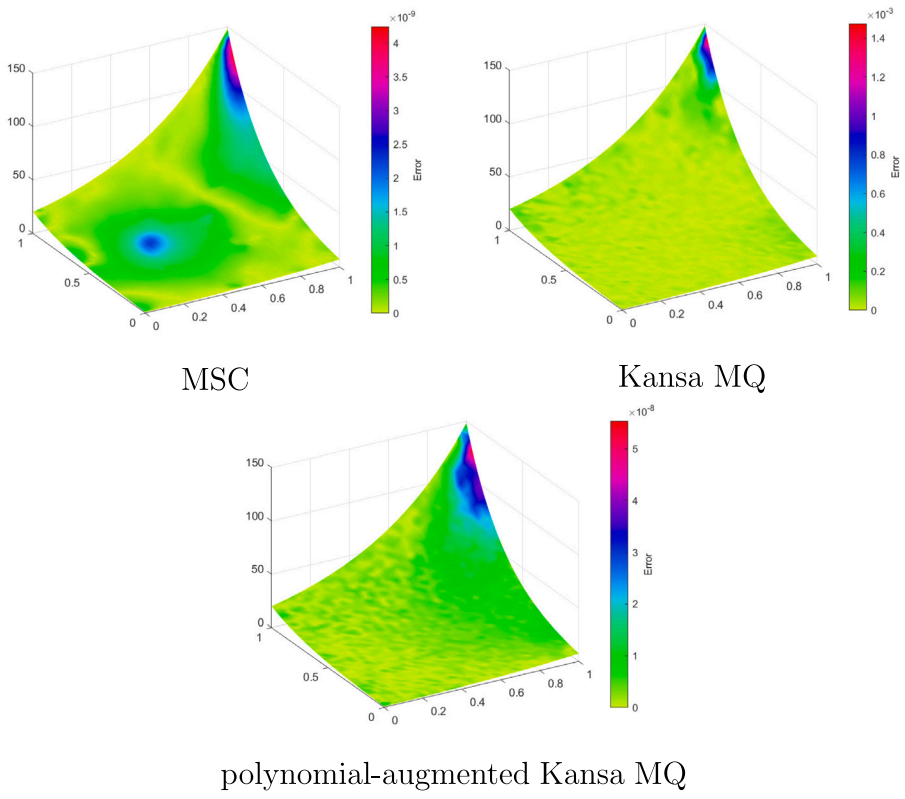

Fig. 16. Error on the surface of the approximated solution for the example presented in Section 5.3. The MSC method, on the top left, is with $r = 11$. The Kansa MQ method with $c = 2.1$ is on the top right and the polynomial-augmented Kansa MQ method, on the bottom, is with $c = 2.1$ and $r = 3$. The simulations use $n_I = 500$ interior points and $n_B = 84$ uniformly distributed boundary points.

Data availability

No data was used for the research described in the article.

Acknowledgments

This research has been achieved as part of RITA "Research ITalian network on Approximation", as part of the UMI group "Teoria dell'Approssimazione e Applicazioni" and was supported by INDAM-GNCS project 2023, UNIPA D26-PREMIO-GRUPPI-RIC-2023, FFR2023. The authors are members of the INdAM research group GNCS.

References

[1] M.J. Gander, F. Kwok, Numerical Analysis of Partial Differential Equations using Maple and MATLAB, Society for Industrial and Applied Mathematics, Philadelphia, PA, 2018.
[2] A.S. Reimer, A.F. Cheviakov, A matlab-based finite-difference solver for the Poisson problem with mixed Dirichlet–Neumann boundary conditions, Comput. Phys. Comm. 184 (3) (2013) 783–798.
[3] H. Wendland, Scattered Data Approximation, in: Cambridge Monographs on Applied and Computational Mathematics, Cambridge University Press, 2004.
[4] M.D. Buhmann, Radial Basis Functions: Theory and Implementations, in: Cambridge Monographs on Applied and Computational Mathematics, Cambridge University Press, 2003.
[5] G.E. Fasshauer, Meshfree Approximation Methods with MATLAB, vol. 6, World Scientific, 2007.
[6] E. Kansa, Multiquadrics—A scattered data approximation scheme with applications to computational fluid-dynamics—II solutions to parabolic, hyperbolic and elliptic partial differential equations, Comput. Math. Appl. 19 (8) (1990) 147–161.
[7] G.E. Fasshauer, M.J. McCourt, Kernel-Based Approximation Methods Using Matlab, vol. 19, World Scientific Publishing Company, 2015.
[8] E. Francomano, M. Paliaga, Highlighting numerical insights of an efficient SPH method, Appl. Math. Comput. 339 (2018) 899–915.
[9] S.A. Sarra, E.J. Kansa, Multiquadric radial basis function approximation methods for the numerical solution of partial differential equations, Adv. Comput. Mech. 2 (2) (2009).
[10] B. Fornberg, N. Flyer, Solving PDEs with radial basis functions, Acta Numer. 24 (2015) 215–258.
[11] M.A. Jankowska, A. Karageorghis, C. Chen, Improved Kansa RBF method for the solution of nonlinear boundary value problems, Eng. Anal. Bound. Elem. 87 (2018) 173–183.

[12] D. Cao, X. Li, H. Zhu, A polynomial-augmented RBF collocation method using fictitious centres for solving the Cahn–Hilliard equation, Eng. Anal. Bound. Elem. 137 (2022) 41–55.
[13] E. Larsson, B. Fornberg, A numerical study of some radial basis function based solution methods for elliptic PDEs, Comput. Math. Appl. 46 (5) (2003) 891–902.
[14] A. Karageorghis, M.A. Jankowska, C.-S. Chen, Kansa-RBF algorithms for elliptic problems in regular polygonal domains, Numer. Algorithms 79 (2018) 399–421.
[15] S. Li, L. Ling, Weighted least-squares collocation methods for elliptic PDEs with mixed boundary conditions, Eng. Anal. Bound. Elem. 105 (2019) 146–154.
[16] A. Karageorghis, C. Chen, X.-Y. Liu, Kansa-RBF algorithms for elliptic problems in axisymmetric domains, SIAM J. Sci. Comput. 38 (1) (2016) A435–A470.
[17] S. Reutskiy, A Novel Semi-Analytic Meshless Method for Solving Two- and Three-Dimensional Elliptic Equations of General Form with Variable Coefficients in Irregular Domains, CMES Comput. Model. Eng. Sci. 99 (4) (2014) 327–349.
[18] E. Kansa, P. Holoborodko, On the ill-conditioned nature of C^{∞} RBF strong collocation, Eng. Anal. Bound. Elem. 78 (2017) 26–30.
[19] F. Dell'Accio, F. Di Tommaso, O. Nouisser, N. Siar, Solving Poisson equation with Dirichlet conditions through multinode shepard operators, Comput. Math. Appl. 98 (2021) 254–260.
[20] F. Dell'Accio, F. Di Tommaso, G. Ala, E. Francomano, Electric scalar potential estimations for non-invasive brain activity detection through multinode Shepard method, in: 2022 IEEE 21st Mediterranean Electrotechnical Conference, MELECON, 2022, pp. 1264–1268.
[21] F. Dell'Accio, F. Di Tommaso, N. Siar, On the numerical computation of bivariate Lagrange polynomials, Appl. Math. Lett. 112 (2021) 106845.
[22] F. Dell'Accio, A. Sommariva, M. Vianello, Random sampling and unisolvent interpolation by almost everywhere analytic functions, Appl. Math. Lett. (2023) 108734.
[23] L. Bos, S. De Marchi, A. Sommariva, M. Vianello, Computing multivariate Fekete and Leja points by numerical linear algebra, SIAM J. Numer. Anal. 48 (5) (2010) 1984–1999.
[24] F. Dell'Accio, F. Di Tommaso, Rate of convergence of multinode Shepard operators, Dolomites Res. Notes Approx. 12 (1) (2019) 1–6.
[25] G.E. Fasshauer, J.G. Zhang, On choosing "optimal" shape parameters for RBF approximation, Numer. Algorithms 45 (2007) 345–368.
[26] R. Cavoretto, A. De Rossi, M.S. Mukhametzhanov, Y.D. Sergeyev, On the search of the shape parameter in radial basis functions using univariate global optimization methods, J. Global Optim. 79 (2021) 305–327.
[27] J. Li, A.H.-D. Cheng, C.-S. Chen, A comparison of efficiency and error convergence of multiquadric collocation method and finite element method, Eng. Anal. Bound. Elem. 27 (3) (2003) 251–257.
[28] Q. Jiang, C. Yao, Z. Ye, C. Zhou, Seepage flow with free surface in fracture networks, Water Resour. Res. 49 (1) (2013) 176–186.
[29] M. Sharan, E. Kansa, S. Gupta, Application of the multiquadric method for numerical solution of elliptic partial differential equations, Appl. Math. Comput. 84 (2) (1997) 275–302.
[30] N. Mai-Duy, T. Tran-Cong, Numerical solution of differential equations using multiquadric radial basis function networks, Neural Netw. 14 (2) (2001) 185–199.
[31] W.F. Hughes, E.W. Gaylord, Basic Equations of Engineering Science, Schaum Publishing Company, New York, 1964.